Journal of Materials Chemistry C

ROYAL SOCIETY OF CHEMISTRY

PAPER

View Article Online
View Journal | View Issue

Cite this: J. Mater. Chem. C, 2023, 11, 10509

A low dielectric constant material synergized by calix[4]arene and benzocyclobutene units†

Chengcheng Zhou, Ding Shen, Xingpeng Chai, Boyang Shi, Wenya Zhu and Guowei Wang *

Received 4th May 2023,
Accepted 6th July 2023

DOI: 10.1039/d3tc01554h

rsc.li/materials-c

The rapid development of the semiconductor industry puts forward higher requirements on the properties of insulating dielectrics. As a supramolecular compound, calix[4]arene has a unique cavity structure, showing potential for a low-*k* material. We herein reported a novel strategy to functionalize the 4-*tert*-butylcalix[4]arene with different numbers of benzocyclobutene (BCB) units (2 or 4) and spacers (–$(CH_2)_3$– or –$(CH_2)_6$–) by sequential substitution and hydrosilylation reactions. These precursors can be cured under heating to form a crosslinked film. The optimized curation condition was screened by differential scanning calorimetry (DSC) measurement. Combining with a comparison experiment using a precursor with calix[4]arene but without BCB units, the wide-angle X-ray scattering (WAXS) pattern and thermal analysis provided solid evidence that the high thermal stability of the film (glass transition temperature (T_g) > 110 °C, 5 wt% loss temperature >367 °C, and the coefficient of the thermal expansion < 87.88 ppm $°C^{-1}$) was majorly contributed by calix[4]arene, while the excellent dielectric properties (the lowest dielectric constant D_k = 2.23 and the average dielectric loss $D_f < 1.5 \times 10^{-3}$) were synergistically affected by both calix[4]arene and BCB units. The static water contact angle was mostly higher than 100° and high hydrophobicity was confirmed, which can meet the additional requirements in practical application. The low dielectric constant synergized by calix[4]arene and the BCB unit is hoped to aid in developing a novel strategy for low-*k* materials.

Introduction

With the rapid development of 5G communication, electronic components are being developed with higher speed and higher integration capacities. However, as the wiring density of a very large-scale integrated circuit (VLSIC) increases, the resistance of metal interconnection wires and the capacitance of interlayer dielectrics in electronic components are prone to form a delay effect called "RC delay", which will cause signal transmission delay, noise interference and power loss.[1–3] The RC delay is closely related to the dielectric constant of the interlayer material, and the use of a material with a low dielectric constant (*i.e.* low-*k* material) can effectively reduce the RC delay. Therefore, the development of low-*k* materials with a low dielectric constant ($D_k < 2.5$) and a low dielectric loss ($D_f < 5 \times 10^{-3}$) is of great value,[2] and has become an important research direction in the field of microelectronics.[4–8]

In recent years, polymeric low-*k* materials with better physical and dielectric properties have gradually replaced the traditional inorganic silica materials.[9] In principle, D_k of polymeric low-*k* materials can be improved by reducing the polarizability of the polymer.[8,10,11] The most typical method is to introduce fluorine atoms into the polymer.[12–14] For example, polytetrafluoroethylene (PTFE) has excellent dielectric properties because the C–F bond in the main chain can effectively reduce the polarity. However, due to the poor thermal properties and tough processability of PTFE, it is difficult to apply PTFE in the field of microelectronics. To make up for this drawback, Wang *et al.* developed a novel fluorinated macromonomer with four trifluoroethylene groups derived from tetraethoxysilane (TEOS) through the Piers–Rubinsztajn reaction, and the precursor can form a flexible and highly transparent free-standing crosslinked polysiloxane film at high temperature, which shows a D_k of 2.58.[11] Additionally, the trifluoromethyl-containing organosiloxanes with cross-linkable styrene groups have also been facilely synthesized, and homopolymerization of these organosiloxanes at high temperature yields polysiloxanes, one of which exhibits a D_k of 2.53.[15]

Alternatively, porous polymeric materials were also developed for low-*k* application ($D_k < 2.0$) because the immobilized air can significantly decrease the D_k.[16–21] For example, Zhang *et al.* synthesized benzocyclobutene-functionalized block copolymers, polycarbosilane-*b*-polylactide (PCBS-*b*-PLA), which

State Key Laboratory of Molecular Engineering of Polymers, Department of Macromolecular Science, Fudan University, Shanghai 200433, China.
E-mail: gwwang@fudan.edu.cn

† Electronic supplementary information (ESI) available. See DOI: https://doi.org/10.1039/d3tc01554h

underwent thermal annealing to produce microphase separation and removal of PLA block to generate nanoporous PCBS with a D_k of 2.11.[21] Similarly, the co-assembly of organosilicate precursors with block copolymer poly(*N*,*N*-dimethylacrylamide)-*b*-poly(lactide) (PDMA-*b*-PLA) produced a film with a D_k of 1.71 and discrete, minimally interconnected pores.[18] Besides, Fu *et al.* reported an alternative approach to crosslinked nanoporous fluoropolymer film *via* surface-initiated atom transfer radical polymerization (ATRP) of pentafluorostyrene (PFS) and divinylbenzene (DVB) on silica nanospheres, and sequential crosslinking of nanospheres and removal of the silica cores, which exhibited a D_k as low as 1.7.[20] However, the precise control of the size and distribution of pores is still a challenge. Moreover, the introduction of pores often reduces the mechanical strength and hydrophobicity of the material, which limits the practical application of porous material in integrated circuits (ICs).

Additionally, it has been reported that introducing bulky groups into the polymer can also effectively reduce the D_k of the material because the bulky units can increase the free volume, weaken the interaction between polymer chains, reduce the density of the polymer, and thus lower D_k.[22–24] For example, some researchers have introduced bulky groups, such as spirobifluorene (D_k = 2.54),[25] adamantane (D_k = 3.39)[26] and polyhedral oligomeric silsesquioxane (POSS) units (D_k = 2.81)[27] into the polymer. However, in most cases, lowering the intrinsic D_k of polymer below 2.5 is challenging. Therefore, it is still meaningful to search for alternative bulky units to reduce the D_k of the polymer.

Calixarene is the third-generation of supramolecular compounds, and has a ring-shaped cavity structure. This compound can coordinate selectively with neutral molecules and ions and self-assemble to form a supramolecular structure. Meanwhile, the cavity size of calixarene can be adjusted by molecular design, and the hydroxyl groups can be readily functionalized. Therefore, calixarene derivatives have considerable application prospects in the fields of materials science, biology, environment, and information.[28–30] For example, some researchers have introduced calixarene into high-temperature resistant thermosetting resins.[31] However, research on calixarene-based low-*k* materials is still absent.

In this contribution, calixarene was employed as a novel bulky group and targeted to the low-*k* material. Aiming to meet the practical requirement of the curation process, and mechanical and dielectric properties, the benzocyclobutene (BCB) units was also combined.[32,33] In detail, 4-*tert*-butylcalix[4]arene functionalized with different numbers of BCB units (2 or 4) and spacers (–$(CH_2)_3$– or –$(CH_2)_6$–) were synthesized by sequential substitution and hydrosilylation reactions (Scheme 1). Calix[4]arene and BCB-based precursors were cured at high temperature, and the thermal stability, hydrophilicity and electric properties of the cured films were carefully investigated by differential scanning calorimetry (DSC), thermogravimetric analysis (TGA), thermomechanical analysis (TMA), dynamic mechanical analysis (DMA), precision impedance analysis, contact angle analysis and wide-angle X-ray scattering (WAXS) measurements. In addition, the calix[4]arene functionalized with allyl groups but without BCB units was cured with dimethylsilyl ether (DMSE) and investigated, which was used as a comparison to discriminate the function of calix[4]arene or BCB units in low-*k* materials.

Experimental section

Materials

4-*Tert*-butylcalix[4]arene (TBCA, 98%, Adamas), tetrabutyl ammonium bromide (TABA, Adamas), chlorodimethylsilane (95%, Adamas), dimethylsilyl ether (DMSE, 98%, Adamas), hexyl bromide (99%, Adamas), 5-hexenyl bromide (96%, Adamas), allyl bromide (99%, Adamas), Karstedt catalyst (in xylene, Pt ~ 2%, Adamas), 4-bromobenzocyclobutene (BCB-Br, 98%, Chemtarget Technologies Co., China) were used as received without further purification. Toluene (99.8%, Aladdin), tetrahydrofuran (THF, 99.5%, Extra Dry, Enemy Chemical Co.), acetonitrile (99.5%, Enemy Chemical Co.), cyclohexane (99.5%, Enemy Chemical Co.) and dichloromethane (DCM, 99.5%, Enemy Chemical Co.) were distilled and stored at 0 °C prior to use. (Benzocyclobutene-4-yl) dimethylsilane (**BCB-SiH**) was synthesized according to the literature.[34] All other reagents were purchased from Enemy Chemical Co. and used as received except for an additional declaration.

Characterization

^{1}H NMR spectra were recorded on a Bruker Avance-400 spectrometer at ambient temperature using $CDCl_3$ as the solvent and tetramethylsilane (TMS) as the internal standard. Matrix-assisted laser desorption ionization time-of-flight (MALDI-TOF) mass spectra were recorded on an AB SCIEX-5800 UltrafleXtreme MALDI TOF/TOF Mass Spectrometer in the positive reflection mode with trans-2-[3-(4-*tert*-butylphenyl)-2-methyl-2-propenylidene]malononitrile (DCTB) as the matrix and sodium trifluoroacetate as the salt. Differential scanning calorimetry (DSC) was performed using a TA Q250 instrument at a heating rate of 10 °C min^{-1} from −20 to 350 °C under a nitrogen flow rate of 50 mL min^{-1}. Thermogravimetric analysis (TGA) was performed on a Mettler Toledo thermal analyzer (A39) under a nitrogen flow rate of 40 mL min^{-1} at a heating rate of 10 °C min^{-1} from 50 to 800 °C. Thermal expansion behaviour and glass transition temperature (T_g) of samples were measured using a Mettler Toledo-SDTA841e thermomechanical analyzer (TMA) performed from −50 to 300 °C at a heating rate of 10 °C min^{-1} under a nitrogen flow rate of 50 mL min^{-1}. Dynamic mechanical analysis (DMA) was carried out on a TA Instrument Q800 by the film stretching mode at a heating rate of 3 °C min^{-1} with the test frequency at 1 Hz from 25 to 300 °C. Fourier Transform Infrared Spectroscopy (FT-IR) was performed on a ThermoFisher Nicolet 6700 spectrometer with KBr pellet and the angle total reflection (ATR) method at room temperature, and the samples were scanned 64 times with wavenumbers ranging from 400 to 4000 cm^{-1}. Dielectric constants and the dielectric loss were investigated by the standard capacitance method on a TongHui TH2839 precision impedance analyzer in a range of frequencies from 50 kHz to 1000 kHz at room temperature. The wide-angle X-ray scattering (WAXS) diffraction patterns of samples were collected on a Xenocs Xeuss

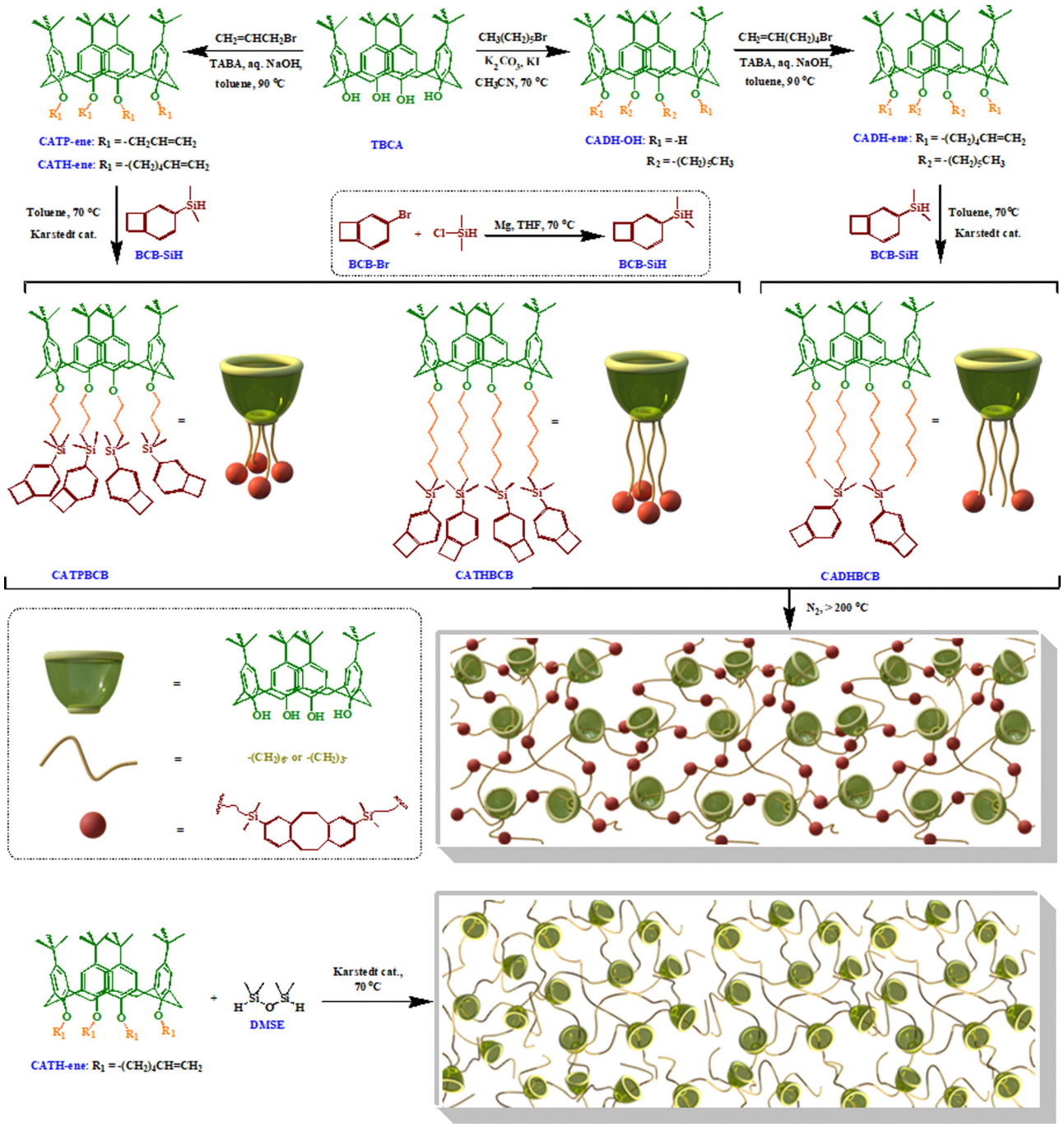

Scheme 1 Schematic illustration of the calix[4]arene and BCB-based precursors, and the curing process.

2.0 scattering system with a Pilatus 3R 200 K-A detector, which was equipped with a CuKα radiation wavelength of 1.54 Å. Static contact angles were obtained using a Dataphysics OCA40 contact angle analyzer at room temperature and ambient humidity.

Synthesis of 4-*tert*-butylcalix[4]arene-25,26,27,28-tetrahexenyl ether (CATH-ene) and 4-*tert*-butylcalix[4]arene-25,26,27,28-tetrapropenyl ether (CATP-ene)

Referring to the literature,[35] **CATH-ene** and **CATP-ene** were synthesized. Using the synthesis of **CATH-ene** as an example, the procedure is illustrated as follows. First, in a 100 mL flask equipped with a magnetic stirrer, a mixture of 4-*tert*-butylcalix-[4]arene (0.65 g, 1.0 mmol), toluene (25.0 mL), 50% w/w NaOH solution (1.0 mL), 5-hexenyl bromide (1.63 g, 10.0 mmol) and TABA (0.03 g, 0.1 mmol) were stirred at 95 °C for 6.0 h. After cooling to room temperature, the reaction was quenched with water (10.0 mL). The organic phase was extracted using ethyl acetate and washed with HCl solution (1.0 M). Then, all the extracts were combined and dried with anhydrous magnesium sulfate (Mg_2SO_4), filtered, and concentrated under vacuum.

The crude product was subjected to flash column chromatography on silica gel with petroleum ether as the eluent affording the product as a brown oil. Similarly, the **CATP-ene** was obtained as a pale-yellow solid by replacing 5-hexenyl bromide with allyl bromide.

CATP-ene. Yield, 91%. ^{1}H NMR (400 MHz, $CDCl_3$, ppm): δ = 6.77 (s, 8H, Ar-**H**), 6.47–6.40 (m, 4H, C***H***═CH_2), 5.28–5.23 (m, 8H, CH═C***H***$_2$), 4.45 (d, 8H, OC***H***$_2$), 4.37 (d, 4H, ArC***H***$_2$Ar), 3.10 (d, 4H, ArC***H***$_2$Ar), 1.08 (s, 36H, –C(C***H***$_3$)$_3$).

CATH-ene. Yield, 82%. ^{1}H NMR (400 MHz, $CDCl_3$, ppm): δ = 6.77 (s, 8H, Ar-***H***), 5.80–5.91 (m, 4H, C***H***═CH_2), 4.96–5.01 (m, 8H, CH═C***H***$_2$), 4.38 (d, 4H, ArC***H***$_2$Ar), 3.85 (t, 8H, OC***H***$_2$), 3.11 (d, 4H, ArC***H***$_2$Ar), 2.12–2.18 (m, 8H, C***H***$_2$–CH═CH_2), 1.99–2.07 (m, 8H, –CH_2C***H***$_2$–), 1.46–1.54 (m, 8H, –C***H***$_2$$CH_2$–), 1.08 (s, 36H, –C(C***H***$_3$)$_3$).

Synthesis of 4-*tert*-butylcalix[4]arene-25,27-dihexyloxy-26,28-dihexyl ether (CADH-ene)

Referring to the literature,[35] **CADH-ene** was synthesized. First, in a 100 mL flask equipped with a magnetic stirrer, a mixture of 4-*tert*-butylcalix[4]arene (0.65 g, 1.0 mmol), potassium carbonate (0.55 g, 4.0 mmol), potassium iodide (0.03 g, 20 mol% of 4-*tert*-butylcalix[4]arene), and acetonitrile (30.0 mL) were refluxed at 85 °C for 30 min. Then, the mixture was cooled to room temperature and hexyl bromide (0.35 g, 2.1 mmol) was added, and the solution was refluxed and monitored using thin-layer chromatography (TLC) (using petroleum ether as the elution). After completion, the solution was cooled, filtered, and evaporated. The residue was dissolved in ethyl acetate and extracted with water. The organic layer was further washed with saturated NaCl solution and dried with anhydrous Mg_2SO_4. Subsequently, the extract was evaporated under reduced pressure and subjected to flash column chromatography on silica gel with petroleum ether as eluent affording the product as white crystals (**CADH-OH**). Finally, the **CADH-ene** was synthesized from **CADH-OH** and 5-hexenyl bromide using a similar procedure as that for the above **CATH-ene**.

CADH-OH. Yield, 94%. ^{1}H NMR (400 MHz, $CDCl_3$, ppm): δ = 7.79 (s, 2H, D_2O exchange, O***H***), 7.03 (s, 4H, Ar-***H***), 6.83 (s, 4H, Ar-***H***), 4.30 (d, 4H, ArC***H***$_2$Ar), 3.96 (t, 4H, OC***H***$_2$), 3.30 (d, 4H, ArC***H***$_2$Ar), 1.98–2.05 (m, 4H, –C***H***$_2$–), 1.62–1.69 (m, 4H, –C***H***$_2$–), 1.36–1.43 (m, 8H, –C***H***$_2$–), 1.27 (s, 18H, –C(C***H***$_3$)$_3$), 0.99 (s, 18H, –C(C***H***$_3$)$_3$), 0.93(t, 6H, –C***H***$_3$).

CADH-ene. Yield, 72%. ^{1}H NMR (400 MHz, $CDCl_3$, ppm): δ = 6.82 (s, 4H, Ar-***H***), 6.74 (s, 4H, Ar-***H***), 5.77–5.95 (m, 2H, C***H*** = CH_2), 4.97–5.07 (m, 4H, CH═C***H***$_2$), 4.40 (d, 4H, ArC***H***$_2$Ar), 3.82–3.89 (m, 8H, OC***H***$_2$), 3.11 (d, 4H, ArC***H***$_2$Ar), 2.14–2.19 (m, 4H, –C***H***$_2$–), 1.99–2.07 (m, 8H, –C***H***$_2$–), 1.46–1.54 (m, 4H, –C***H***$_2$–), 1.35–1.41 (m, 12H, –C***H***$_2$–), 1.12 (s, 18H, –C(C***H***$_3$)$_3$), 1.05 (s, 18H, –C(C***H***$_3$)$_3$), 0.94(t, 6H, –C***H***$_3$).

Synthesis of 4-*tert*-butylcalix[4]arene-25,26,27,28-tetrahexyloxy benzocyclobutene (CATHBCB), 4-*tert*-butylcalix[4]arene-25,27-dihexyloxy-26,28-dihexyloxy benzocyclobutene (CADHBCB) and 4-*tert*-butyl- calix[4]arene-25,26,27,28-tetrapropoxy benzocyclobutene (CATPBCB)

The **CATHBCB**, **CADHBCB** and **CATPBCB** were synthesized by a hydrosilylation reaction. Using the synthesis of **CATHBCB** as an example and the procedure is illustrated as follows. First, into a 100 mL Schlenk flask equipped with a magnetic stirring bar, **CATH-ene** (0.98 g, 1.0 mmol), 25.0 mL of dried toluene, and three drops of Karstedt catalyst were sequentially added. Then, the mixture was stirred in an ice bath under nitrogen and continued for 30 minutes. Subsequently, **BCB-SiH** (1.30 g, 8.0 mmol) was added dropwise into the Schlenk flask for 30 minutes. After the addition, the temperature was increased to 70 °C and the reaction was further carried out for 8.0 h. After removing the solvents by rotary evaporation, the mixture was purified by a silica gel column using petroleum ether as the eluent and precipitated by methanol. The targeted **CATHBCB** was collected as a colourless liquid. Similarly, **CADHBCB** and **CATPBCB** were also obtained as a colourless liquid from **CADH-ene** or **CATP-ene** and **BCB-SiH**.

CATHBCB. Yield, 92%. ^{1}H NMR (400 MHz, $CDCl_3$, ppm): δ = 7.36 (d, 4H, Ar-**H**), 7.21 (s, 4H, Ar-**H**), 7.05 (d, 4H, Ar-**H**), 6.78 (s, 8H, Ar-H), 4.39 (d, 4H, ArC***H***$_2$Ar), 3.81 (t, 8H, OC***H***$_2$), 3.18 (s, 16H, –C***H***$_2$–), 3.10 (d, 4H, ArC***H***$_2$Ar), 1.95–2.04 (m, 8H, –C***H***$_2$–), 1.34–1.47 (m, 24H, –C***H***$_2$–), 0.76–0.80 (t, 8H, –C***H***$_2$–), 1.09 (s, 36H, –C(C***H***$_3$)$_3$), 0.24 (d, 24H, –C***H***$_3$). MALDI-TOF *m*/*z* for [M·Na]$^+$ found: 1650.6.

CADHBCB. Yield, 89%. ^{1}H NMR (400 MHz, $CDCl_3$, ppm): δ = 7.36 (d, 2H, Ar-***H***), 7.21 (s, 2H, Ar-***H***), 7.02 (d, 2H, Ar-***H***), 6.81 (s, 4H, Ar-***H***), 6.75 (s, 4H, Ar-***H***), 4.40 (d, 4H, ArC***H***$_2$Ar), 3.77–3.87 (m, 8H, OC***H***$_2$), 3.18 (s, 8H, –C***H***$_2$–), 3.10 (d, 4H, ArC***H***$_2$Ar), 1.97–2.08 (m, 8H, –C***H***$_2$–), 1.35–1.44 (m, 24H, –C***H***$_2$–), 1.13 (s, 18H, –C(C***H***$_3$)$_3$), 1.08 (s, 18H, –C(C***H***$_3$)$_3$), 0.76–0.80 (t, 4H, –C***H***$_2$–), 0.95(t, 6H, –C***H***$_3$), 0.27 (d, 12H, –C***H***$_3$). MALDI-TOF *m*/*z* for [M·Na]$^+$ found: 1328.9.

CATPBCB. Yield, 84%. Propyl chain is too short to inhibit the overturning of calix[4]arenes in hydrosilylation. The overturning led to the abnormal splitting of the nuclear magnetic spectrum (Fig. S2, ESI†). MALDI-TOF *m*/*z* for [M·Na]$^+$ found: 1482.6.

General procedure for the curation of CATHBCB, CADHBCB or CATPBCB

Typically, a solution of calix[4]arene and BCB-based precursors (**CATHBCB**, **CADHBCB** or **CATPBCB**) (100 mg mL^{-1} in DCM) was first coated into an aluminium mold (25.0 × 30.0 mm, cylinder). Then, the solvent was naturally evaporated, and the aluminium mold was put into a tubular furnace and heated at 210 °C for 1.0 h, 230 °C for 1.0 h, and 250 °C for 2.0 h under a nitrogen atmosphere. After cooling to room temperature, the aluminium mold was chemically corroded and demolded with dilute hydrochloric acid (1.0 M HCl) affording the cured film. The film was washed with ionized water and dried under vacuum at 60 °C for 6.0 h. Finally, the film was polished into discs with a diameter of 20.0 mm for further characterization.

General procedure for the curation of CATH-ene with DMSE

Typically, **CATH-ene** (0.98 g, 1.0 mmol) was dissolved in 20.0 mL of dried cyclohexane in a 100 mL flask equipped with a magnetic stirrer, and two drops of Karstedt's catalyst were added at 0 °C. Then, DMSE (0.27 g, 2.0 mmol) was added dropwise into the flask under a nitrogen atmosphere and

stirred for 30 minutes. After that, the solution was coated into an aluminium mold (25.0 × 30.0 mm, cylinder) and the solvent was slowly evaporated in a vacuum oven at room temperature. Then, the temperature was elevated to 70 °C and the sample was cured as a film. Finally, the film was cut into discs with a diameter of 20.0 mm for further characterization.

Results and discussion

Synthesis and characterization of calix[4]arene and BCB-based precursors

As shown in Scheme 1, in the presence of NaOH/TBAB, the hydroxyl groups on 4-*tert*-butylcalix[4]arene were subjected to a substitution reaction with 5-hexenyl bromide, and the fully substituted calix[4]arene-based intermediate (**CATH-ene**) with terminal unsaturated –CH═CH_2 groups was obtained. Subsequently, **CATH-ene** was subjected to a hydrosilylation reaction with **BCB-SiH** in the presence of a Karstedt catalyst and the precursor of **CATHBCB** containing both calix[4]arene and BCB units was achieved. Similarly, **CATPBCB** was synthesized by a substitution reaction of 4-*tert*-butylcalix[4]arene with allyl bromide, and further a hydrosilylation reaction with **BCB-SiH**. Alternatively, the disubstituted calix[4]arene-based intermediates (**CADH-OH**) can be obtained by changing the catalyst system and the equivalent of bromoalkene to 4-*tert*-butylcalix[4]arene in the substitution reaction. **CADH-OH** was further reacted with hexyl bromide for **CADH-ene**, which was subjected to a hydrosilylation reaction with **BCB-SiH** for **CADHBCB**.

The precursors of **CATHBCB**, **CATPBCB** and **CADHBCB** were comprehensively characterized using ^{1}H NMR spectra and MALDI-TOF mass spectra, respectively (Fig. 1, Fig. S1 and S2, ESI†). Using the ^{1}H NMR spectrum for **CATHBCB** as an example (Fig. 1a–c), the disappearance of resonance signals for protons on vinyl groups (5.92–5.81 ppm) and silicon hydrogen (4.51 ppm), as well as the retention of characteristic resonance signals for protons on calix[4]arene (4.37–4.40 ppm) and BCB (3.28 ppm) units, demonstrated the success of substitution and hydrosilylation reactions. However, when allyl bromide was employed in a substitution reaction, the irregular splitting in the ^{1}H NMR spectrum for **CATPBCB** indicated that the configuration inversion of calix[4]arene occurred (Fig. S2, ESI†). This phenomenon did not happen in the case with 5-hexenyl bromide, in which the complete "cone"-shaped product was actually obtained. The reason can be attributed to the introduction of a relatively longer spacer (–$(CH_2)_6$–) in **CATHBCB**, which tended to prevent the configuration inversion in calix[4]arene. In Fig. 1d–f, the MALDI-TOF mass spectra of **CADHBCB**, **CATPBCB** and **CATHBCB** clearly show the measured molecular weights of 1328.9, 1482.6 and 1650.6, which are rather consistent with the calculated values. The MALDI-TOF mass spectra combined with the ^{1}H NMR spectra provided solid evidence that the calix[4]arene and BCB-based precursors were successfully synthesized.

Curation of calix[4]arene and BCB-based precursors

The literature had shown that the BCB units can be cured under high temperature (>200 °C).[36] Aiming to define the optimized curing condition, the thermo-polymerization process of the precursors was first monitored by differential scanning calorimetry (DSC) (Fig. 2) and Fourier transform infrared (FT-IR) spectroscopy (Fig. S3, ESI†) measurements, respectively. As can be seen from Fig. 2, **CATHBCB**, **CADHBCB** and **CATPBCB** share the same onset curing temperature (~225 °C) and exothermic peak temperature (~260 °C), respectively. The normalized exothermic enthalpy of both **CATHBCB** and **CATPBCB** was ~260 J g^{-1}, while that for **CADHBCB** was ~140 J g^{-1}. The discrepancy was consistent with the difference in the content of

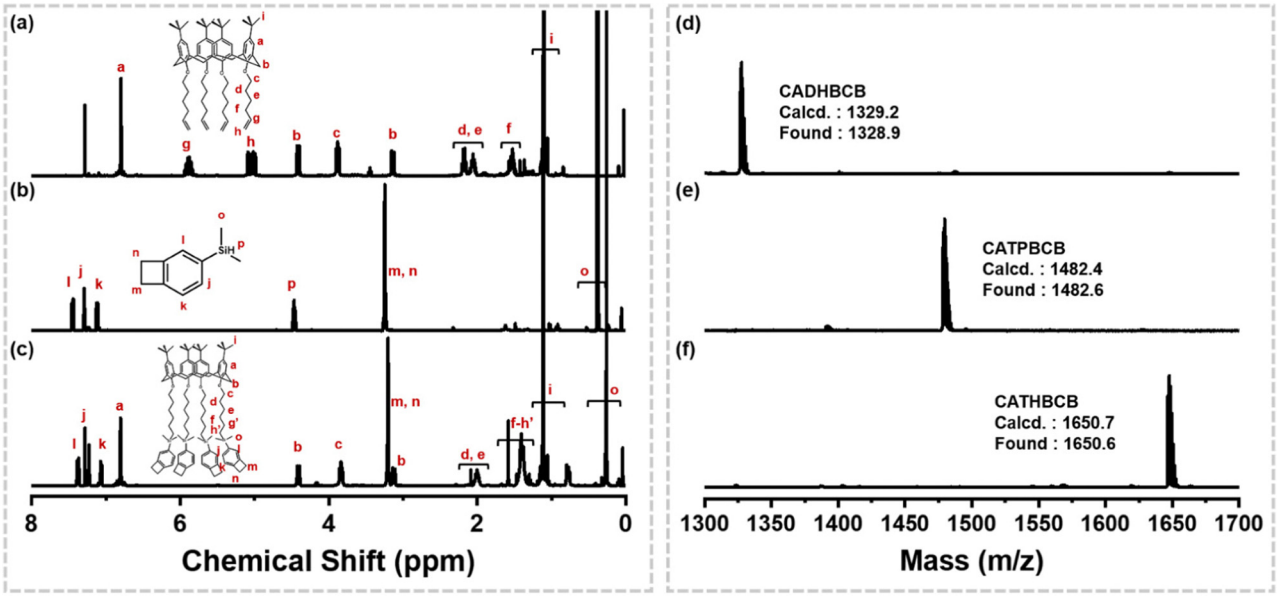

Fig. 1 ^{1}H NMR spectra of (a) CATH-ene, (b) BCB-SiH, and (c) CATHBCB. MALDI-TOF mass spectra of (d) **CADHBCB**, (e) **CATPBCB** and (f) **CATHBCB**. All the samples show peaks of $[M{\cdot}Na]^+$ corresponding to the calculated molecular weights.

BCB units on the corresponding precursors. The weight percentages of the BCB units in **CATHBCB**, **CADHBCB** and **CATPBCB** were 25.3%, 28.2% and 15.8%, respectively. From the FT-IR spectra shown in Fig. S3 (ESI†), the typical absorbance centered at 1467 cm^{-1} and 930 cm^{-1} was attributed to the C–H in-plane deformation and the C–H stretching vibration of methylene in a four-membered ring of BCB. After the curation process, these signals disappeared. Correspondingly, the absorbance peaked at 1459 cm^{-1} represented the C–H bending vibration of methylene in alkyl chains, which existed in both precursors and polymers. Thus, the DSC and FT-IR spectra results demonstrated the complete curation of the precursors. Based on the DSC results, the following curation process was performed in a tubular furnace, which was programmed at 210 °C for 1.0 h, 230 °C for 1.0 h, and 250 °C for 2.0 h under a nitrogen atmosphere to ensure the complete curing of the precursors.

Dielectric properties of the cured films from calix[4]arene and BCB-based precursors

As the dielectric properties of the materials were the main target in this work, the dielectric constant (D_k) and dielectric loss (D_f) of the cured films in the frequency range of 50–1000 kHz were measured by an impedance analyzer at room temperature. From Fig. 3, it can be discriminated that the average D_k and D_f of cured **CATHBCB** was 2.23 and 1.3×10^{-3}. The cured **CATPBCB** and **CADHBCB** also showed quite excellent dielectric properties with an average D_k of 2.30 and 2.44, and an average D_f lower than 1.3×10^{-3}, respectively. These D_k values were distinctly lower than those for the commercial low-*k* resins CYCLOTENE® (D_k was 2.7) and many recently reported low-*k* materials such as fluoropolymers,[11,37] modified polyimides[7] and other BCB-based resins.[25,38] Alternatively, in the absence of the cured BCB units in the comparative experiment, the average D_k and D_f of cured **CATH + DMSE** were 2.51 and 1.1×10^{-3}, respectively, which were higher than those for the cured **CATHBCB**, **CATPBCB** and **CADHBCB**. However, D_k of 2.51 was obviously lower than that for the typical PDMS resin ($D_k \approx 2.8$). Based on these results, it can be concluded that the extremely low D_k of the cured **CATHBCB** should be contributed by the synergistic effect of calix[4]arene and cured BCB units.

In order to unveil the function of calix[4]arene and cured BCB units on the improved dielectric properties, according to

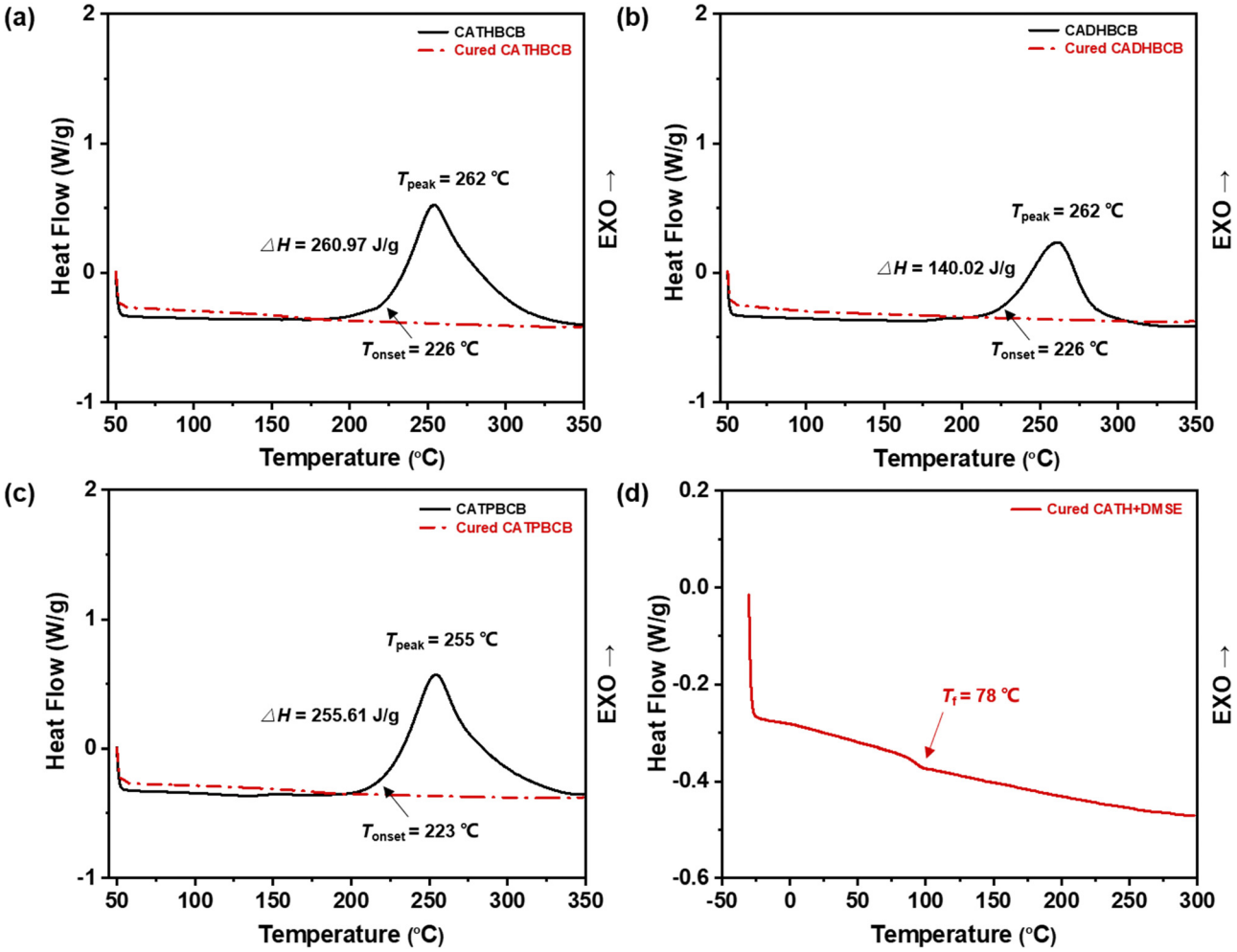

Fig. 2 DSC traces of (a) **CATHBCB** and cured **CATHBCB**, (b) **CADHBCB** and cured **CADHBCB**, (c) **CATPBCB** and cured **CATPBCB**, (d) cured **CATH + DMSE** at a heating rate of 10 °C min^{-1} under nitrogen atmosphere.

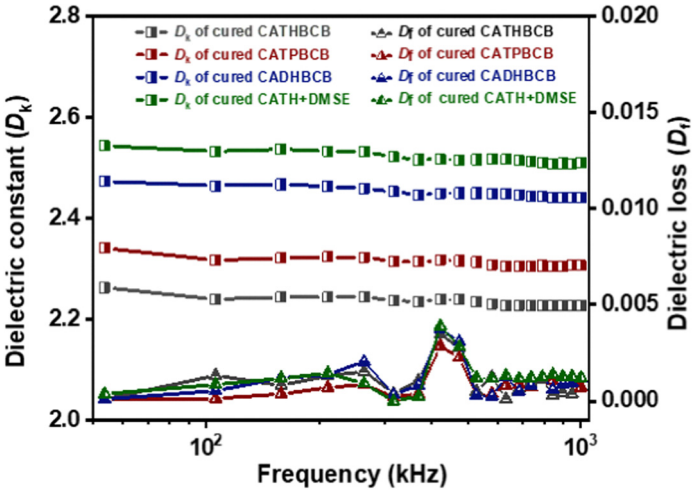

Fig. 3 Dielectric constant (D_k, square) and dielectric loss (D_f, triangle) of cured **CATHBCB** (grey), cured **CADHBCB** (red), cured **CATPBCB** (blue) and cured **CATH + DMSE** (green) under different frequencies at room temperature.

the literature,[39] wide-angle X-ray scattering (WAXS) was used to characterize the micro-structures of the cured films. In our work, the WAXS patterns of the cured **CATHBCB**, **CADHBCB**, **CATPBCB** and **CATH + DMSE** showed continuous swelling peaks instead of sharp diffraction peaks, which meant there were a series of nanopores with a continuous pore size distribution in the films (Fig. 4). From Fig. 4a, it can be observed that the peak absorption of cured **CATHBCB**, **CADHBCB**, **CATH + DMSE** was majorly concentrated at 2θ = 8.5° and 18.3°, and two average pore sizes in the films can be derived as about 1.051 nm and 0.487 nm by the Bragg equation. By comparing the WAXS patterns for **CATHBCB**, **CADHBCB** and **CATH + DMSE**, it can be deduced that the nanopores in the material were mostly derived from calix[4]arenes rather than the cured BCB units. From Fig. 4b, it can be observed that the peak absorption of cured **CATPBCB** was centered at 7.2° and 16.8°, and the corresponding nanopore size was calculated at about 1.226 nm and 0.527 nm. The position of the peaks was slightly different from those of the above **CATHBCB** and **CADHBCB**. The configuration inversion of calix[4]arenes due to shorter alkyl spacer (–$(CH_2)_3$–) can be presumed to be the main factor. Thus, the WAXS results confirmed that there were a large number of nanopores in the cured films. Correspondingly, these nanopores led to a low density of a material, which explains the extremely low D_k.

Thermal stability of the cured films from calix[4]arene and BCB-based precursors

The thermodynamic properties of cured **CATHBCB**, **CADHBCB** and **CATPBCB** were investigated using DSC and TGA measurements. As shown in Fig. 5(a), the TGA measurement was performed under a nitrogen atmosphere and the thermal decomposition behaviour of cured products was investigated. The cured **CATHBCB** showed a 5.0 wt% loss temperature (T_{5d})

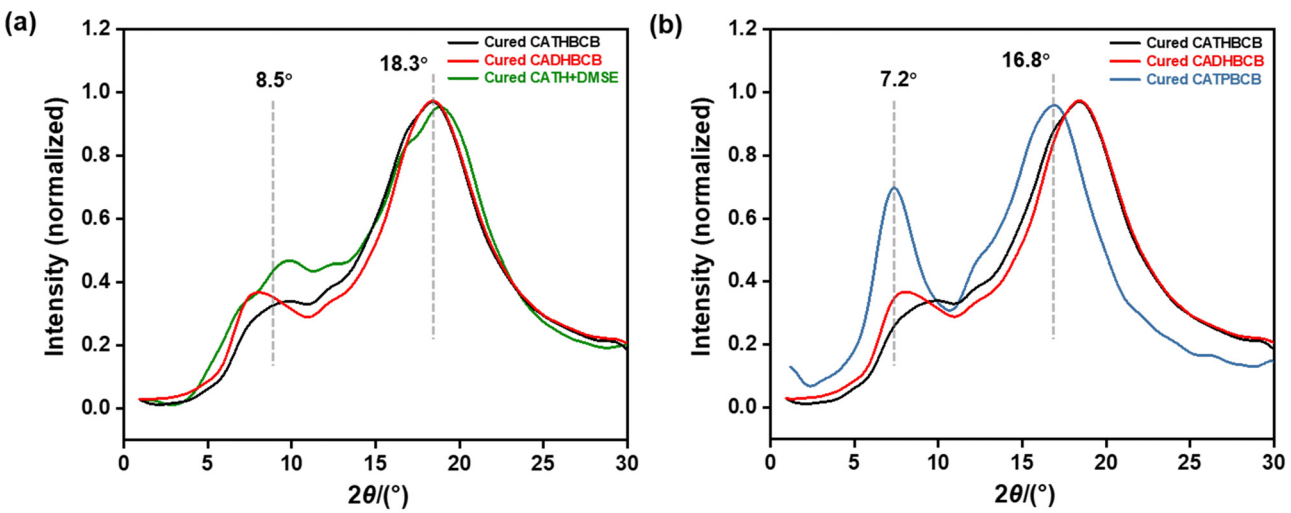

Fig. 4 The WAXS patterns of (a) cured **CATHBCB** (black), cured **CADHBCB** (red) and cured **CATH + DMSE** (green), (b) cured **CATHBCB** (black), cured **CADHBCB** (red) and cured **CATPBCB** (blue) with a scanning rate of 0.5° min^{-1}.

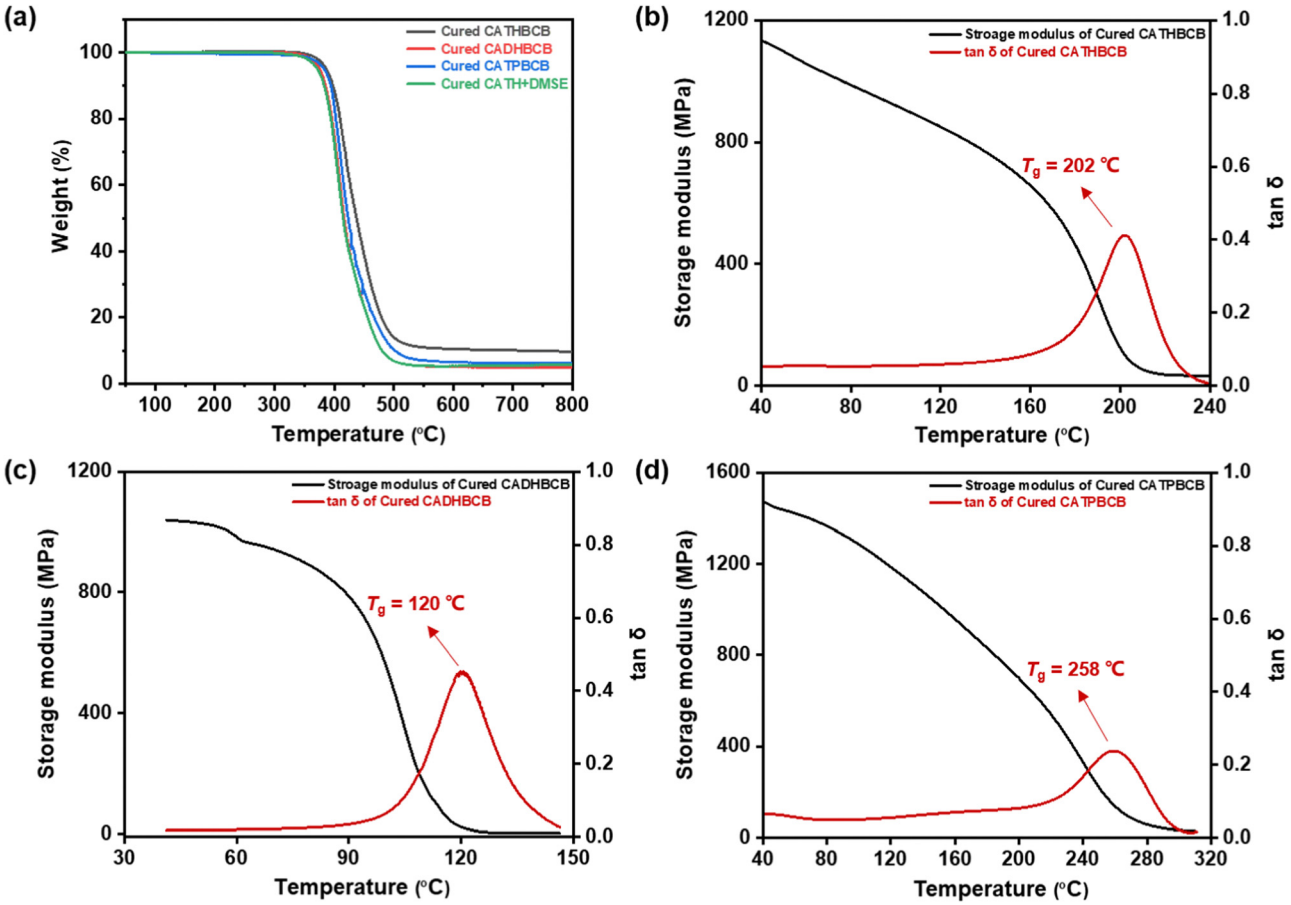

Fig. 5 (a) TGA traces of cured **CATHBCB** (black), cured **CADHBCB** (red), cured **CATPBCB** (blue) and cured **CATH + DMSE** (green) with a ramping rate of 10 °C min^{-1} under nitrogen atmosphere. DMA traces of (b) cured **CATHBCB**, (c) cured **CADHBCB** and (d) cured **CATPBCB** at a heating rate of 3 °C min^{-1} under nitrogen atmosphere.

of 387 °C and a residue of 10.1% at 800 °C. The cured **CADHBCB** had a T_{5d} of 367 °C and a residue of 4.9% at 800 °C. The cured **CATPBCB** had a T_{5d} of 383 °C and a residue of 6.2% at 800 °C. The TGA results showed that the cured samples can meet the general application requirements of ICs. Meanwhile, it can be proved that the increase in the number of BCB units can effectively improve thermal stability. For the cured **CATH + DMSE**, which had a T_{5d} of 337 °C and a residue of 5.8% at 800 °C (Fig. 5a), the thermal stability was similar to the cross-linked polydimethylsiloxane (PDMS) reported in lirerature.[40] From Fig. 2a–c, in the temperature range from 50 °C to 350 °C, the DSC traces of cured **CATHBCB**, **CADHBCB** and **CATPBCB** showed no endothermic/exothermic peaks, which indicated the complete curation of the BCB units in the corresponding precursors. As a comparison, the DSC trace of cured **CATH + DMESE** (Fig. 2d) revealed a glass transition temperature (T_g) at about 78 °C.

DMA was carried out to investigate the mechanical properties of the materials. The storage modulus and tan δ are shown in Fig. 5b–d. The cured **CATHBCB**, **CADHBCB** and **CATPBCB** exhibited storage moduli of 1.15 GPa, 1.04 GPa, and 1.49 GPa, respectively, at room temperature. According to the change of tan δ with temperature, T_{gs} of cured **CATHBCB**, **CADHBCB** and **CATPBCB** were 202 °C, 120 °C and 258 °C, respectively. Compared with the cured **CADHBCB** (Fig. 5b), the cured **CATHBCB** (Fig. 5c) has higher thermodynamic stability, which can be attributed to the higher content of the BCB units in the corresponding precursor. Additionally, the cured **CATPBCB** with a shorter alkyl spacer (–$(CH_2)_3$–) also showed a significantly increased T_g (Fig. 5d). Therefore, it can be demonstrated that shortening the alkyl spacers and increasing the content of the BCB units in the calix[4]arene and BCB based precursors can effectively improve the mechanical properties and thermal properties of the cured films.

For practical IC applications, dimensional stability is also an important factor, which can be characterized by TMA under a nitrogen atmosphere from −50 °C to 300 °C (Fig. 6). The results showed that all the cured calix[4]arene and BCB-based materials showed similar thermal expansion behaviour over the employed temperature range. The coefficient of thermal expansion (CTE) values of cured **CATHBCB**, cured **CADHBCB** and cured **CATPBCB** were determined to be 87.88 ppm $°C^{-1}$, 81.52 ppm $°C^{-1}$ and 85.19 ppm $°C^{-1}$, respectively (Fig. 6a–c). These results were close to the reported CTE of epoxy resins in printed circuit board (PCB) system.[2,41] The T_{gs} of cured **CATHBCB**, cured **CADHBCB** and cured **CATPBCB** were 211 °C, 110 °C and 233 °C, respectively, which were consistent with the T_{gs} obtained from DMA

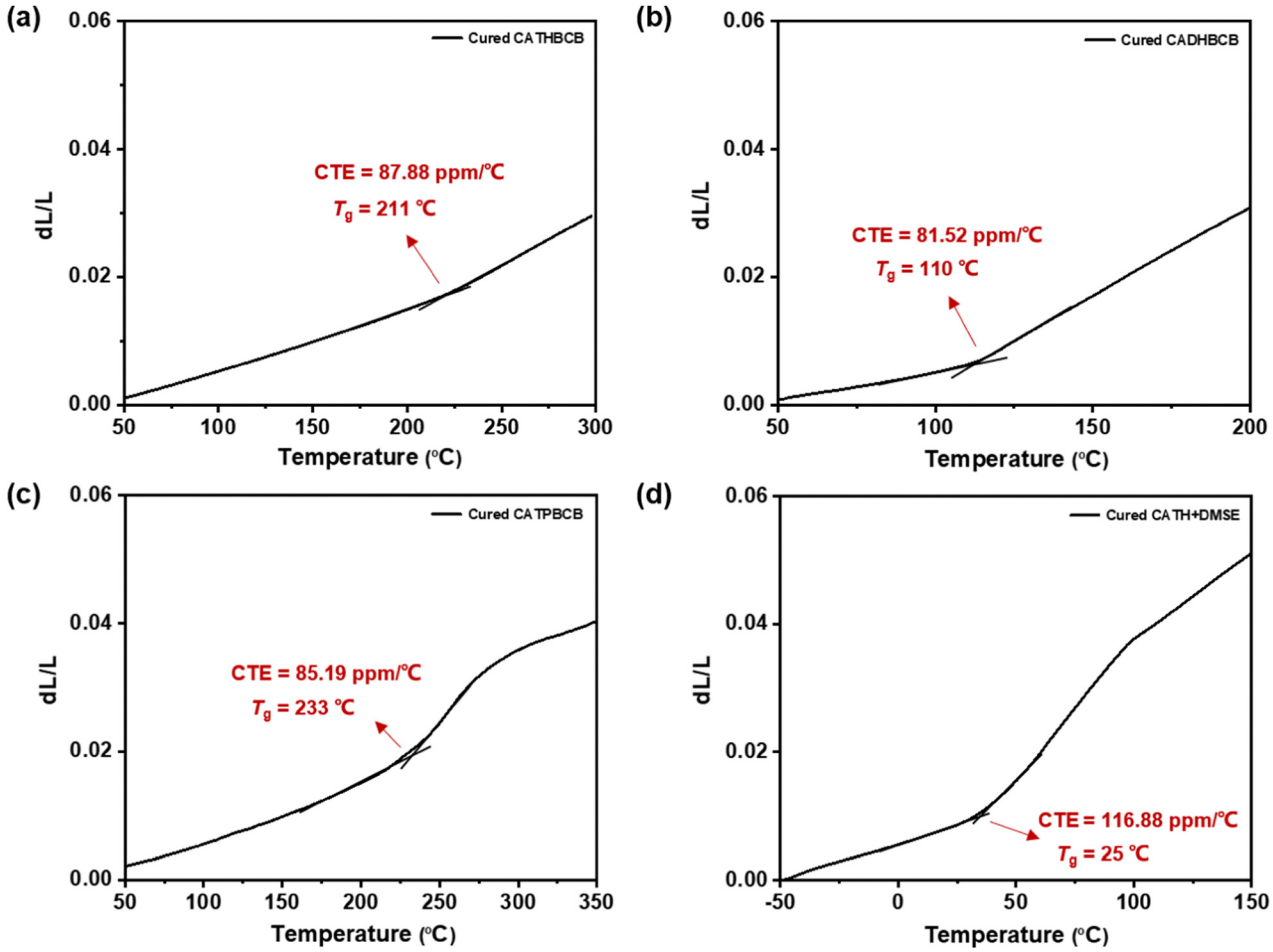

Fig. 6 TMA traces of (a) cured **CATHBCB**, (b) cured **CADHBCB**, (c) cured **CATPBCB** and (d) cured **CATH + DMSE** with a heating rate of 10 °C min^{-1} under nitrogen atmosphere.

characterization. Compared with the above films containing calix[4]arene and cured BCB units, the cured **CATH + DMSE** exhibited a lower T_g (~ 35 °C) and a slightly higher CTE value (116.88 ppm $°C^{-1}$) (Fig. 6d). In this case, the BCB units was absent. Again, it can be clearly discriminated that the introduction of BCB units can significantly improve the thermal properties of the cured system. It should be mentioned that T_g of the cured **CATHBCB**, **CADHBCB** and **CATPBCB** cannot be discriminated from the DSC curves (Fig. 2a–c), the reason might be attributed to the highly crosslinked and rigid network in films. In this case, the response on the heat capacity was too weak to be discriminated. Alternatively, in the TMA and DMA measurements, the deformation mutation of the samples can be readily detected in a wide range, and T_g can be thus derived.

Hydrophobic properties of the cured films

Furthermore, high hydrophobicity is also essential for an interlayer insulating dielectric material, as water absorption will lead to a sharp decrease in both the dielectric and mechanical properties of the material. Thus, the static water contact angle measurement was further performed to assess the hydrophobicity of the material. The films of **CATHBCB**, **CADHBCB**, **CATPBCB** and **CATH +**

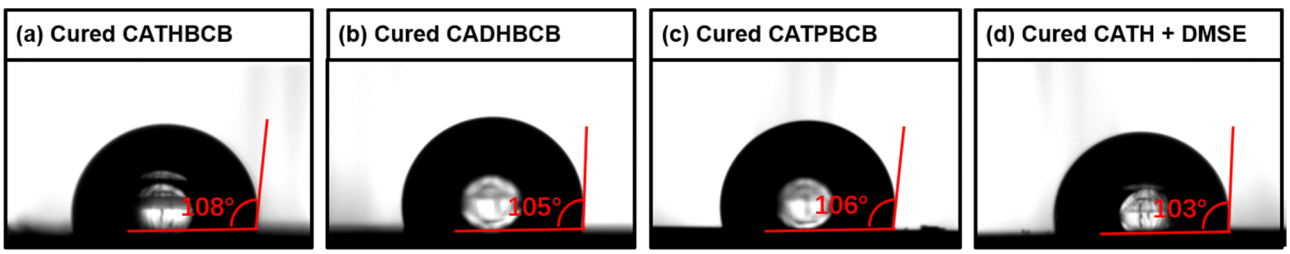

Fig. 7 Static water contact angle of (a) cured **CATHBCB**, (b) cured **CADHBCB**, (c) cured **CATPBCB** and (d) cured **CATH + DMSE** on a silicon wafer.

DMSE cured on silicon wafers exhibited static water contact angles of 108°, 105°, 106°and 103°, respectively (Fig. 7). The results showed that the cured films maintained good hydrophobicity, which can meet the general requirements in practical IC applications.[42]

Conclusions

In summary, starting from 4-*tert*-butylcalix[4]arene, several calix[4]arene-based precursors modified with multiple BCB units were successfully synthesized by substitution and hydrosilylation reactions. These calix[4]arene and BCB-based precursors (**CATHBCB**, **CADHBCB**, and **CATPBCB**) were capable of self-curing at high temperature. Alternatively, the **CATH** + **DMSE** was cured and used as a comparison to confirm the function of 4-*tert*-butylcalix[4]arene and BCB units. The results showed that all calix[4]arene and BCB-based films exhibited excellent thermal stability, dimensional stability, and hydrophobicity. In particular, the cured film from **CATHBCB** containing one calix[4]arene and four BCB units had an extremely low D_k of 2.23 and a D_f of 1.3×10^{-3}. This work presented a novel low-*k* material based on calix[4]arene and BCB units, which demonstrated great potential and prospect as interlayer insulating dielectrics.

Conflicts of interest

There are no conflicts to declare.

Acknowledgements

We appreciate the financial support of this research by the National Natural Science Foundation of China (21774022 and 22271058).

Notes and references

1 P. A. Kohl, in *Annual Review of Chemical and Biomolecular Engineering*, ed. J. M. Prausnitz, 2011, vol. 2, pp. 379–401.
2 G. Maier, *Prog. Polym. Sci.*, 2001, **26**, 3–65.
3 K. Maex, M. R. Baklanov, D. Shamiryan, F. Iacopi, S. H. Brongersma and Z. S. Yanovitskaya, *J. Appl. Phys.*, 2003, **93**, 8793–8841.
4 X. Y. Zhao and H. J. Liu, *Polym. Int.*, 2010, **59**, 597–606.
5 J. R. Hou, L. X. Fang, G. Huang, M. L. Dai, F. P. Liu, C. Y. Wang, M. H. Li, H. Zhang, J. Sun and Q. Fang, *ACS Appl. Polym. Mater.*, 2021, **3**, 2835–2848.
6 E. K. Carlson, *Engineering-PRC*, 2020, **6**, 725–727.
7 C. Qian, R. X. Bei, T. W. Zhu, W. W. Zheng, S. W. Liu, Z. G. Chi, M. P. Aldred, X. D. Chen, Y. Zhang and J. R. Xu, *Macromolecules*, 2019, **52**, 4601–4609.
8 W. Volksen, R. D. Miller and G. Dubois, *Chem. Rev.*, 2010, **110**, 56–110.
9 C. B. Cheng, R. H. Fan, Z. Y. Wang, Q. Shao, X. K. Guo, P. T. Xie, Y. S. Yin, Y. L. Zhang, L. Q. An, Y. H. Lei, J. E. Ryu, A. Shankar and Z. H. Guo, *Carbon*, 2017, **125**, 103–112.
10 F. K. He, K. K. Jin, J. J. Wang, Y. J. Luo, J. Sun and Q. Fang, *Macromol. Chem. Phys.*, 2015, **216**, 2302–2308.
11 J. J. Wang, J. F. Zhou, K. K. Jin, L. Wang, J. Sun and Q. Fang, *Macromolecules*, 2017, **50**, 9394–9402.
12 Y. Q. Wang, J. Sun, K. K. Jin, J. J. Wang, C. Yuan, J. W. Tong, S. Diao, F. K. He and Q. Fang, *RSC Adv.*, 2014, **4**, 39884–39888.
13 S. Tian, J. Sun, K. K. Jin, J. J. Wang, F. K. He, S. J. Zheng and Q. Fang, *ACS Appl. Mater. Interfaces*, 2014, **6**, 20437–20443.
14 K. Tsuchiya, Y. Shibasaki, M. Aoyagi and M. Ueda, *Macromolecules*, 2006, **39**, 3964–3966.
15 F. Liu, X. Chen, L. Fang, J. Sun and Q. Fang, *Polym. Chem.*, 2020, **11**, 6163–6170.
16 D. Grosso, C. Boissiere and C. Sanchez, *Nat. Mater.*, 2007, **6**, 572–575.
17 M. Seino, W. D. Wang, J. E. Lofgreen, D. P. Puzzo, T. Manabe and G. A. Ozin, *J. Am. Chem. Soc.*, 2011, **133**, 18082–18085.
18 T. M. Hermans, J. Choi, B. G. G. Lohmeijer, G. Dubois, R. C. Pratt, H. C. Kim, R. M. Waymouth and J. L. Hedrick, *Angew. Chem., Int. Ed.*, 2006, **45**, 6648–6652.
19 G. D. Fu, Z. L. Yuan, E. T. Kang, K. G. Neoh, D. M. Lai and A. C. H. Huan, *Adv. Funct. Mater.*, 2005, **15**, 315–322.
20 G. D. Fu, Z. H. Shang, L. Hong, E. T. Kang and K. G. Neoh, *Adv. Mater.*, 2005, **17**, 2622–2626.
21 S. B. Zhang, H. Hu, H. T. Yu, Y. W. Huang and J. X. Yang, *Macromol. Res.*, 2017, **25**, 381–385.
22 M. R. Wang, Rusli, M. B. Yu, N. Babu, C. Y. Li and K. Rakesh, *Thin Solid Films*, 2004, **462**, 219–222.
23 C. M. Lew, Z. J. Li, S. Li, S. J. Hwang, Y. Liu, D. I. Medina, M. W. Sun, J. L. Wang, M. E. Davis and Y. S. Yan, *Adv. Funct. Mater.*, 2008, **18**, 3454–3460.
24 K. Zhang, L. Han, P. Froimowicz and H. Ishida, *Macromolecules*, 2017, **50**, 6552–6560.
25 L. X. Fang, J. F. Zhou, C. Q. He, Y. Q. Tao, C. Y. Wang, M. L. Dai, H. Y. Wang, J. Sun and Q. Fang, *Polym. Chem.*, 2020, **11**, 2674–2680.
26 L. Q. Kong, Y. R. Cheng, Y. X. Jin, T. K. Qi and F. Xiao, *J. Appl. Polym. Sci.*, 2016, **133**, 43456.
27 Y. Y. Deng, D. L. Zhou, D. Han, Q. Zhang, F. Chen and Q. Fu, *Compos. Sci. Technol.*, 2020, **189**, 108035.
28 C. G. Bezzu, M. Helliwell, B. M. Kariuki and N. B. McKeown, *J. Porphyrins phthalocyanines*, 2011, **15**, 686–690.
29 J. Wang, X. Ding and X. Guo, *Adv. Colloid Interface Sci.*, 2019, **269**, 187–202.
30 V. S. Sharma, V. K. Vishwakarma, P. S. Shrivastav, A. A. Sudhakar, A. S. Sharma and P. A. Shah, *ACS Omega*, 2022, **7**, 45752–45796.
31 M. Wang, Y. Ning, K. Zhou, T. Su and Z. Wang, *Thermosetting Resin*, 2018, **33**, 1–5.
32 Y. L. Yu, X. N. Dong, K. Zhao, J. C. Cheng and J. Y. Zhang, *Surf. Coat. Technol.*, 2010, **205**, 205–212.
33 J. Y. Li, Z. Y. Zhang, T. W. Zhu, Z. Li, J. Wang and Y. R. Cheng, *Eur. Polym. J.*, 2020, **126**, 109502.
34 D. L. Zhou, J. H. Li, Q. Y. Guo, X. Lin, Q. Zhang, F. Chen, D. Han and Q. Fu, *Adv. Funct. Mater.*, 2021, **31**, 2102074.

35 I. Bitter, A. Grun, B. Agai and L. Toke, *Tetrahedron*, 1995, **51**, 7835–7840.
36 M. Dai, Y. Tao, L. Fang, C. Wang, J. Sun and Q. Fang, *ACS Sustainable Chem. Eng.*, 2020, **8**, 15013–15019.
37 C. Yuan, K. K. Jin, K. Li, S. Diao, J. W. Tong and Q. Fang, *Adv. Mater.*, 2013, **25**, 4875–4878.
38 Y. Feng, K. Jin, J. Guo and C. Wang, *Polym. Chem.*, 2021, **12**, 4812–4821.
39 Z. Wang, H. Wang, P. Ren and M. Wang, *J. Macromol. Sci. A*, 2019, **56**, 794–802.
40 S. Ansari, J. M. Varghese and K. R. Dayas, *Polym. Adv. Technol.*, 2009, **20**, 459–465.
41 H. J. Hwang, S. W. Hsu, C. L. Chung and C. S. Wang, *React. Funct. Polym.*, 2008, **68**, 1185–1193.
42 Y. L. Cheng, K. W. Leon, J. F. Huang, W. Y. Chang, Y. M. Chang and J. Leu, *Microelectron. Eng.*, 2014, **114**, 12–16.